Impact of updated traffic emissions on HONO mixing ratios simulated for urban site in Houston, Texas

Beata H. Czader, Yunsoo Choi, Xiangshang Li, Sergio Alvarez, Barry Lefer

Department of Earth and Atmospheric Sciences, University of Houston, Houston, USA

Correspondence to: B.H. Czader (bczader@uh.edu)

Abstract

Recent measurements in Houston show that HONO traffic emissions are 1.7% of NO_x emissions which is about twice the previously estimated value of 0.8% based on tunnel measurements in 2001. The 0.8% value is widely used to estimate mobile emissions of HONO for air quality modeling applications. This study applies the newly estimated HONO/NO_x ratio in the WRF-SMOKE-CMAQ modeling system and estimates the impact of higher HONO traffic emissions on its mixing ratios. Since applied emission inventory resulted in overestimates of NO_x mixing ratios and because HONO emissions and chemical formation depends on the magnitude of NO_x, thus, before proceeding with HONO emission modifications emissions of NO_x were adjusted to reflect current emission trends. The modeled mixing ratios of NO_x were evaluated against measured data from a number of sites in the Houston area. Overall, the NO_x mean value dropped from 11.11 ppbv in the base case to 7.59 ppbv in the NO_x adjusted case becoming much closer to the observed mean of 7.76 ppbv. The Index of Agreement (IOA) is improved in the reduced NO_x case (0.71 vs. 0.75) and the Absolute Mean Error (AME) is lowered from 6.76 to 4.94. The modeled mixing ratios of HONO were evaluated against the actual observed values attained at the Moody Tower in Houston. The model could not reproduce the morning HONO peaks when the low HONO/NO_x ratio of 0.008 was used to estimate HONO emissions. Doubling HONO emissions from mobile sources resulted in higher mixing ratios, the mean value increased from 0.30 ppbv to 0.41 ppbv becoming closer to the observed mean concentrations of 0.69 but still

low; AME was slightly reduced from 0.46 to 0.43. IOA for simulation that used the 2001 emission values is 0.63 while for simulation with higher HONO emission it increased to 0.70. Increased HONO emissions from mobile sources resulted in 14% increase in OH during morning time at the location of the Moody Tower and 3% when averaged over urban area. The increase calculated for daytime was 7% and 1% for the Moody Tower and the urban area, respectively. The impact on ozone was found to be marginal. This study results shed light on the underestimated HONO and OH in the morning from global/regional chemical transport models with the typical emission of 0.8% HONO emission out of the total NO_x emissions.

1. Introduction

Photolysis of nitrous acid (HONO) is an important source of hydroxyl radical (OH). OH plays a crucial role in the oxidation of volatile organic compounds (VOCs) leading to the formation of ozone and secondary organic particulate matter. Main sources of OH are photolysis of ozone, formaldehyde, alkenes, and nitrous acid (Elshorbany et al., 2009; Mao et al., 2010; Kim et al., 2014). Photolysis of ozone and formaldehyde are the most important sources of OH during mid-day and afternoon hours; however, the highest contribution to radical production during early morning hours comes from photolysis of HONO (e.g. Perner and Platt, 1979; Harris et al., 1982; Czader et al., 2012, 2013).

HONO can be either formed through chemical reactions or emitted to the atmosphere from combustion processes. Among the most known chemical sources of HONO is the gas-phase formation from the reaction between OH and nitric oxide (NO) (Pagsberg et al., 1997) and the heterogeneous formation on surfaces from the hydrolysis of nitrogen dioxide (NO_2) (Kleffmann et al., 1998; Finlayson-Pitts et al., 2003). Other chemical sources of HONO are described elsewhere (Kleffmann et al., 2005, 2007; George et al. 2005; Stemmler et al. 2006, 2007; Crowley and Carl, 1997; Li et al., 2008, 2009; Carr et al., 2009; Amedro et al., 2011). Emissions of HONO from traffic were estimated by Kirchstetter et al. (1996) and Kurtenbach et al. (2001) who performed tunnel studies and reported exhaust emission ratio of HONO to NO_x in a range of 0.003-0.008. The value of 0.008 is used in the Community Multiscale Air Quality (CMAQ)

model to calculate HONO emissions from mobile sources (Foley et al., 2010) as well as in other models, for example, in a box model employed to study HONO sources in Houston (Wong et al. 2013). The relative contribution of HONO emissions from traffic to other sources when using the HONO to NO_x ratio of 0.008 is about 9% based on simulations for eastern U.S. (Sarwar et al. 2008). For high NO_x areas in China Li et al. (2011) calculated as high as 26% contribution of HONO emissions to its total sources but they could not reproduce the high morning peak values of HONO associated with traffic emissions. Czader et al. (2012) studied HONO formation for Houston conditions and also applied the 0.008 HONO/NO_x ratio to estimate HONO emissions. In addition to default sources of HONO present in CMAQ they implemented photolytic HONO formation; however, on many occasions the peak morning values continued to be underpredicted by the model. Recent measurements performed in Houston in 2009 show that the observed HONO/NO_x emission ratio is 0.017 (Rappenglueck et al., 2013), which is about twice as high as previously reported and implemented in CMAQ modeling system. The impact of using higher HONO emissions in air quality modeling applications has not been evaluated. Therefore, in this work HONO emissions from mobile sources will be doubled to reflect the newly reported HONO/NO_x emission ratio and the impact of higher HONO traffic emissions on its mixing ratios will be estimated in the WRF-CMAQ modeling system. The impact of increased HONO on the OH and O_3 will also be investigated in this study.

Because in air quality applications HONO is derived from the total NO_x reported in an emission inventory and chemical formation of HONO is directly related to NO and NO_2 mixing ratios; therefore, HONO predictions by air quality models depend on how well the model captures emissions of NO_x. Czader et al. (2012) pointed out that the correlation between measured and simulated HONO values increased significantly when data points with wrong NO_2 prediction were ignored and only data for which NO_2 values were simulated within 70% of the measured value were considered. Therefore, accurate estimation of NO_x in air quality models is crucial to properly simulate HONO mixing ratios. Previous studies used remote sensing and in-situ surface observations to analyze accuracy of NO_x emissions and indicated that the National Emission Inventory (NEI) has large uncertainty in emissions in urban areas (Choi et al., 2012; Choi, 2014). Of particular, Choi (2014) issued that both NEI2005 and NEI2008 have significant NO_x

overestimates in Houston. Thus, in this study, before proceeding with modifications of HONO emissions, NO_x emissions will be adjusted using the U.S. Environmental Protection Agency (EPA) annual trend values and the absolute amounts of simulated surface NO_x concentrations will be evaluated.

2. Methodology

Meteorological parameters were derived with the Weather Research and Forecasting (WRF) model version 3.5 (Skamarock et al., 2008). NCEP North American Regional Reanalysis (NARR) data provided by the NOAA/OAR/ESRL PSD (available at http://www.esrl.noaa.gov/psd/) were utilized to initialize WRF simulations. The 2008 National Emission Inventory (NEI2008) generated by the Environmental Protection Agency (EPA) was processed with the Sparse Matrix Operator Kernel Emissions (SMOKE) system to obtain gridded, chemically and temporally resolved emission files ready to use in an air quality model. The air quality simulations were performed with the three-dimensional Community Multiscale Air Quality (CMAQ) model (Byun and Schere, 2006) version 5.0.1 with the Carbon Bond 05 chemical mechanism and aerosol 5 module (cb05tucl_ae5_aq).

Simulations were performed for a domain with 4 km grid resolution covering southeast Texas, with 84 grid cells in east-west direction, 66 grid cells in south-north direction, and 27 vertical layers. The boundary conditions were obtained from the University of Houston air quality forecasting system (http://spock.geosc.uh.edu) from a larger domain with 12 km grid resolution, 150 grid cells in east-west direction and 134 grid cells in south-north direction. Initial conditions were also obtained from the air quality forecasting results from the nested south-east Texas domain. Simulations were performed for the month of September 2013 during which the DISCOVER-AQ campaign took place in Houston providing many different meteorological and chemical measurements that can be utilized for model evaluation.

2.1 Adjusting NO_x and HONO emissions

Previous studies used remote sensing and in-situ surface observations to analyze accuracy of NO_x emissions and pointed to the fact that the National Emission Inventory (NEI) has large uncertainties in emissions for urban areas (Choi et al., 2012; Choi, 2014). Of particular, Choi (2014) issued that both NEI2005 and NEI2008 might have significant overestimates of NO_x emissions in Houston even with the consideration of the uncertainties caused from other chemical and physical processes. Adequate estimation of NO_x emissions is critical for properly predicting HONO mixing ratios.

Since our simulations employed NEI2008 there was a need of adjusting emissions to reflect conditions of 2013. In this study, instead of relying on the remote-sensing-derived data or surface-measured data to adjust an emission inventory (e.g., Kim et al., 2009; Kim et al., 2011; Choi et al., 2012; Choi, 2014) we use the long-term trends of anthropogenic NO_x emission reported by U.S. EPA. Then the impact of the adjusted NO_x emissions on surface NO_x concentrations is evaluated by comparing the simulated and observed NO_x concentrations. According to EPA, emissions of nitrogen oxides from anthropogenic sources were reduced between 2008 and 2013. Table 1 shows emission values based on the EPA trends (available at: http://www.epa.gov/ttn/chief/trends/index.html#tables) for on-road mobile sources and other anthropogenic sources excluding wildfires. Relatively to values for the year 2008 there was 28% reduction in on-road mobile NO_x emissions on a nationwide scale and 20% reduction in other anthropogenic NO_x emissions in year 2013. To follow the emissions trends we created a sensitivity case in which on-road NO_x emissions were reduced by 30% and anthropogenic point source emissions were reduced by 20%.

NEI provides emission rates for nitrogen oxides, during the processing with SMOKE NO_x emissions for mobile sources are separated into 90% NO, 9.2% NO_2, and 0.8% HONO. However, Rappenglueck et al. (2013) reports much higher HONO contribution from mobile sources in Houston; based on all measurements HONO traffic emissions are 1.7% of NO_x emissions which is about twice the previously estimated value of 0.8% based on tunnel measurements in 2001. The HONO/NO_x ratio reported by Kurtenbach et al. (2001) is based on

measurements performed between 6 am and 2 pm, for both weekdays and weekends where 22 200 ± 400 vehicles were passing on weekdays and 13 300 ± 1 400 cars passing on weekends. The vehicle fleet was composed of 6.0% heavy-duty trucks, 6.0% commercial vans, 12% diesel and 75% gasoline powered passenger cars, and 1.0% motorcycles. The ratio calculated by Rappenglueck et al. (2013) is based on measurements performed during weekdays reflecting high traffic, early morning conditions (4-8 am). The measurements were performed at highway junction in Houston with very high traffic load (about 400 000 vehicles passing daily), which is much larger than that in the tunnel study. The vehicle fleet was represented by 93-95% of gasoline fueled vehicles and 5-7% by diesels during the morning hours. Another difference between these two studies is in vehicle speed, with a typical speed of 50-90 km/h in the tunnel studies and much lower speed during the morning peak traffic hours in Houston. To reflect the latest values of HONO emissions measured in Houston in air quality modeling additional sensitivity case was created in which contribution of HONO from mobile sources was doubled at the cost of NO_2. The following speciation was used for the sensitivity case: 90% NO, 8.4% NO_2, and 1.6% HONO. It is worth to note that since the newly reported ratio reflects high traffic conditions during morning rush hours on weekdays our model sensitivity study provides estimate of the upper bound of the impact of HONO emissions on pollutant levels in urban areas.

The following three simulations cases are performed and analyzed in this study:
B – base case, with NO_x emissions rates obtained from NEI2008 and $HONO/NO_x = 0.008$;
N – reduced emissions of NO_x case: mobile sources * 0.7, point sources * 0.8; $HONO/NO_x = 0.008$;
NH – similar as N but with doubled HONO emissions from mobile sources, this is $HONO/NO_x=0.016$.

2.2 Measurements

Measured values from the Continuous Ambient Monitoring Stations (CAMS) system, operated by the Texas Commission on Environmental Quality (TCEQ), were utilized for evaluating NO_x emission inventory. During the time period of interest 30 stations inside our 4 km modeling

172 domain reported NO_x measurements. Figure 1 show location of sites in the Houston – Galveston
173 metropolitan area, where color of the symbol indicates the measured mean NO_x mixing ratios
174 during the month of September 2013. Several sites, such as 78, 84, 618, 619, and 1016 have low
175 mean values; those sites reflect regional and/or suburban conditions. Couple sites, such as 26 and
176 53, have medium range NO_x values reflecting urban air mixture dominated by traffic emissions.
177 Many sites close to highways or in downtown Houston and east of downtown are exposed to
178 heavy traffic as well as a combination of traffic and industrial emissions. They have very high
179 NO_x mean values; those are CAMS sites 1, 8, 114, 403, 408, 411 and the Moody Tower (MT)
180 site described below.

181

182 The Moody Tower, located east of downtown, was designated as a "super" site during air quality
183 study campaigns in Houston in years 2006 (Lefer and Rappenglück, 2010) and 2009 (Olaguer et
184 al., 2013) during which many chemical and meteorological measurements were taken. During
185 September 2013 measurements at the Moody Tower complimented the DISCOVER-AQ
186 campaign. The measurements were taken at 60 m a.g.l. In addition to NO_x and ozone, HONO
187 was also measured on several days during the month of September 2013.

188

189 **3. Results**

190

191 **3.1 Evaluation of NO_x modeling**

192

193 Table 2 shows summary of statistical parameters of modeled NO_x mixing ratios for the base case
194 (B) and the reduced NO_x case (N) as compared to measured values at CAMS sites, where R is
195 the Pearson coefficient, AME – absolute mean error calculated as:

$$AME = \left(\frac{1}{n}\right)\sum_{1}^{n}|C_m - C_o|$$

"n" is the number of data points, “m” corresponds to modeled values and “o” to observed ones;

IOA – index of agreement, calculated according the following equation:

$$IOA = 1 - \frac{\sum_1^n (C_m - C_o)^2}{\sum_1^n \left(|C_o - \tilde{O}| + |C_m - \tilde{O}|\right)^2}$$

“$\tilde{O}$” corresponds to observed mean value. Compared to a Pearson coefficient the index of agreement is a more comprehensive measure of how well the concentrations are predicted since it takes into account not only scattering of data but also biases (Willmott, 1981).

Statistical parameters were calculated for all available data pairs from CAMS sites inside the modeling domain. The measured mean value from all sites is 7.76 ppbv, the simulated mean value dropped from 11.11 ppbv in the base case to 7.59 ppbv in the reduced NO_x case becoming closer to the observed mean. Both, R and IOA are improved in the reduced NO_x case (R=0.58, IOA = 0.71 in the base case, R=0.59, IOA = 0.75 in the reduced NO_x case) and AME is lowered from 6.76 ppbv to 4.94 ppbv. Overall, the reduced NO_x simulation case gives better NO_x prediction in comparison to the base case. When looking at individual stations affected by emissions from different sources the improvement from NO_x reductions is beneficial for most of sites, but leads to underpredictions at several sites. Many stations with medium range NO_x mixing ratios, such as CAMS 35 and 53 show improvement from NO_x reduction. There are also cases when NO_x continue to be too high even after reduction of emissions. This is the case for CAMS sites 26 and 78 that represent sub-urban conditions with low measured NO_x mixing ratios (usually below 10 ppb) and low mean values of 5.61 and 3.29, respectively. The model represents them as urban sites with significant traffic signature and therefore with much higher than measured mixing ratios. Even though in our study we adjusted NO_x emissions to reflect emission reduction between the year 2008 and 2013 some overpredictions may occur since, as pointed by Choi (2014), NO_x rates in the base 2008 inventory might be too high. Very high NO_x mixing ratios are recorded in areas with heavy traffic and close to industrial facilities in the

eastern part of Houston; such as at CAMS stations 1, 403, 411, and 416. NO_x mixing ratios at those stations were heavily overpredicted and consequently those stations benefit the most from NO_x reductions as presented in Figure 2. Our results are similar to the previous study by Choi (2014) who issued that NO_x mixing ratios at urban regions are overpredicted by air quality models, but NO_x at the rural regions are underpredicted.

The Moody Tower site served as a super site for couple of measurements campaigns in Houston and many different chemical and meteorological parameters were measured there, including NO, NO_2, and HONO. It is located in close proximity to downtown and major highways and is affected by quite high NO_x emissions. Figure 3 shows comparison of measured at the Moody Tower and simulated mixing ratios of NO (top) and NO_2 (bottom). Again, two simulation cases are compared: the case with regular emissions as included in NEI2008 (B) and the reduced NO_x emissions case (N). It can be seen that for both compounds the peak values were overpredicted by the base case while reduced NO_x case resulted in lower mixing ratios making them closer to the observed values. In particular, NO mixing ratios are much better predicted by reduced NO_x emissions case. Both, NO_2 morning peaks and low range day and nighttime NO_2 values, although lowered, continue to be overpredicted most of the time.

3.2 HONO modeling

Since reduction of NO_x emissions resulted in better prediction of NO_x mixing ratios at the Moody Tower and nearby areas this case was used as a base for testing impact of increased HONO emissions. Figure 4 shows changes in HONO emissions rates between the sensitivity case in which $HONO/NO_x=0.016$ (indicated as NH) and the base case that used $HONO/NO_x=0.008$ (indicated as N). Doubling HONO emissions resulted in up to 0.01 mole/s increase in emission rates from mobile sources along highways. Figure 5 show differences in simulated mixing ratios of HONO for morning conditions at 7 a.m. LT that corresponds to the time of the highest HONO emissions from traffic and the highest HONO mixing ratios. The left panel shows results for the surface layer. It can be seen that changes in HONO mixing ratio at the surface occur along highways following the pattern of emission changes presented in Figure

4. Differences in HONO mixing ratios at the second modeled layer, which corresponds to measurements taken at the Moody Tower, are shown in the right panel of Figure 5. At this level the air is mixed and the spatial signature of mobile emissions diminishes.

HONO is not routinely measured in Houston; in spite of that, during September 2013 HONO was measured at the Moody Tower to compliment measurements during DISCOVER-AQ campaign. However, the measurements were not continuous and the data are limited to several days. Figure 6 shows timeseries of measured and simulated HONO mixing ratios at the Moody Tower. The mixing ratios obtained from the reduced NO_x simulation case (N), for which the $HONO/NO_x$ emission ratio of 0.008 was used, are much lower than observed HONO values. The values from the increased HONO case (NH), with the $HONO/NO_x$ emission ratio of 0.016, are higher, especially the morning peaks, and closer to the observations. The statistical parameters for HONO modeling at the Moody Tower are presented in Table 3. The mean value increased from 0.30 in the base case to 0.41 ppbv in the increased HONO emissions case but continue to be lower than the observed mean of 0.69 ppbv. The index of agreement increased from 0.63 to 0.70 indicating benefits of increased HONO emissions. Clearly, improvement in HONO peak values can be seen on September 12, 18, 23, 24, 25 and 30, especially on September 12 the model with increased HONO emissions nicely follow HONO peak while the case with low $HONO/NO_x$ emission rates resulted in underprediction of the peak value. However; as pointed by Czader et al. (2012) HONO predictions depends on how well the model captures NO_x concentrations, especially NO_2, since heterogeneous HONO formation is directly related to NO_2 concentrations and greatly influences morning HONO mixing ratios. It can be seen that overprediction of NO and NO_2 on September 11, 19, and 24 leads to overprediction of HONO. We can conclude that misprediction of precursors is responsible for HONO misprediction and expect that if NO_x mixing ratios for those days are accurately simulated also HONO values would be close to observation. This is not a case on September 18 when, despite the fact that NO is well predicted and NO_2 overpredicted, HONO peak is underpredicted. The reasoning for that is unknown, but it is probably due to the uncertainties in other HONO sources. Also, variations of simulated HONO mixing ratios from day to day are influenced not only by emissions but also by other parameters, for example, the model capabilities to predict grow of the mixing layer and wind fields as well as

clouds that influence photolysis rates. To more clearly present differences between the two simulated cases (N and NH) and measured data we calculated the average diurnal profiles of HONO and presented them in Figure 7. The modeled profiles follow the measured one showing high peak in the morning and low values during a daytime. It can be seen that the NH scenario, in which higher emission ratio was utilized, improves HONO morning peaks. Since only HONO emissions from mobile sources were increased it is expected to see the largest differences in mixing ratios during early morning times when the traffic emissions are the highest, the mixing layer height low allowing for accumulation of HONO, and photochemistry not very active. It is worth to note that all available measured data for HONO for September 2013 are from weekdays and the higher $HONO/NO_x$ ratio measured in Houston was also calculated based on measurements taken during weekdays. The model underprediction during daytime can be explained by the fact that the default model version that we used in this study does not account for the photochemical HONO sources. Also, too low modeled average profile during daytime is caused by underpredictions of HONO on Sep. 23-25 which can be attributed to stronger modeled winds in comparison to weak observed winds causing modeled HONO to be removed from the observational site.

The photolysis of HONO is a source of hydroxyl radical. Figure 8 shows a snapshot of spatial pattern of OH mixing ratios (left) and differences in OH mixing ratios (right) between simulations with increased HONO emissions (NH) and regular emissions with 0.008 $HONO/NO_x$ emissions ratio (N) for September 12, which is a day with nicely predicted HONO mixing ratios. An increase in OH occurs along highways corresponding to increased HONO mobile emissions. Based on the 1 month of simulated surface concentrations the average increase in HONO due to doubling its emissions from mobile sources is 36% at the location of the Moody Tower and 10% when averaged over the urban area. The average increase in the morning OH (between 6 – 8 a.m. LT) is 14% at the location of the Moody Tower and 3% when averaged over the urban area. The ozone increase is below 1% for both the Moody Tower and the urban area. The average increase in OH during daytime (6 a.m. – 8 p.m. LT) is 7% for the Moody Tower and 1% for the urban area. The increase in ozone is again below 1%. Since HONO emissions from mobile sources that peak in the morning were modified therefore, it is understandable that the impact of these additional HONO emissions on OH and ozone is higher during morning time than afternoon hours. To obtain more insights on the fate of HONO we performed additional

312 model simulations in which we utilized the process analysis that provides information on
313 chemical and physical processes influencing pollutant mixing ratios. The analysis was performed
314 for the Moody Tower site for Sep. 10-13, 2013. At the surface, at the location of the Moody
315 Tower the average contribution of vertical transport to the loss of HONO is 77%, horizontal
316 transport contributes 8%, chemical removal 11 % and dry deposition 5%. HONO mixing ratios
317 along with process affecting changes in mixing ratios for the second model layer, which
318 corresponds to the altitude of measurements, are presented in Figure 9. It can be seen that
319 transport (horizontal and vertical) continue to be a dominant loss process at this altitude
320 contributing on average 77% to the total HONO loss while chemical loss contributes only 23%
321 to the total loss. The chemical loss of HONO is dominant only during couple of morning hours.
322 This explains the fact that even though HONO mixing ratios significantly increased upon
323 additional emissions, HONO was removed mainly by transport with only small portions taking
324 part in chemical reactions converting it to OH and furthermore to O_3.

325

326 **4. Summary**

327 The WRF - SMOKE - CMAQ modeling system was used for evaluation and adjustment of NO_x
328 emissions. In particular, HONO/NO_x emission ratio from mobile sources was increased and its
329 impact on HONO mixing ratios as well as on OH and O_3 was evaluated.

330 First, NO_x emissions were adjusted to reflect emission trends. Simulations with adjusted NO_x
331 emissions resulted in overall better NO_x prediction as mixing ratios become closer to measured
332 values. The average NO_x mean value from all analyzed sites dropped from 11.11 ppbv to 7.59
333 ppbv and is much closer to the observed mean of 7.76 ppbv, IOA is improved in the reduced
334 NO_x case (0.71 vs. 0.75) and the AME is lowered from 6.76 to 4.94. Therefore, the reduced NO_x
335 case was taken as a base for adjusting HONO emissions according to values measured in
336 Houston.

337

338 Doubling HONO emission from mobile sources and therefore making them closer to the newly
339 reported HONO/NO_x ratio of 0.017 resulted in increased HONO mixing ratios especially during

morning peak values. Based on 1 month of simulated data 36% increase in HONO mixing ratio at the location of the Moody Tower was obtained from the case with higher emission ratios utilized in simulation. The increase in HONO values averaged over the urban area was 10%. Simulated HONO mixing ratios were compared to vales measured at the Moody Tower. The mean value increased from 0.30 ppbv in the base HONO emission case to 0.41 ppbv in the increased HONO emission case and become closer to the observed mean of 0.69, but still low. The index of agreement for simulation that used the 2001 HONO/NO_x emission ratio of 0.008 is 0.63 while for the simulation with doubled HONO emissions IOA increased to 0.70. Increased HONO emissions from mobile sources resulted in 14% increase in OH during morning time at the location of the Moody Tower and 3% when averaged over urban area. The increase calculated for daytime was 7% and 1% for the Moody Tower and the urban area, respectively. The impact on ozone was found to be marginal (below 1%).

This study results could shed light on the underestimated HONO in the morning from global/regional chemical transport model with the typical emission ratio of 0.8% HONO emission out of the total NO_x emissions. In addition, since HONO is the major radical source in the morning (e.g., Perner and Platt, 1979; Harris et al., 1982; Czader et al., 2013), underpredictions of HONO would lead to underprediction of OH radical.

Acknowledgements. The authors would like to thank the Texas Air Research Center (TARC) for supporting this work. They are also thankful to Lijun Diao for help in setting up WRF and to Hyuncheol Kim for helping with CAMS dataset.

References

Amedro, D., Parker, A. E., Schoemaecker, C., and Fittschen, C.: Direct observation of OH radicals after 565 nm multi-photon exAmedro, D., Parker, A. E., Schoemaecker, C., and Fittschen, C. Direct observation of OH radicals after 565 nm multi-photon excitation of NO_2 in the presence of H2O, Chem. Phys. Lett., 513, 12–16, doi:10.1016/j.cplett.2011.07.062, 2011.

Byun, D. and Schere, K. L.: Review of the Governing Equations, Computational Algorithms, and Other Components of the Models-3 Community Multiscale Air Quality (CMAQ) Modeling System, Appl. Mech. Rev., 59, 51–77, 2006.

Carr, S., Heard, D. E., and Blitz, M. A.: Comment on "Atmospheric Hydroxyl Radical Production from Electronically Excited NO_2 and H_2O", Science, 324, 336b, doi:10.1126/science.1166669, 2009.

Choi, Y. 2014: The impact of satellite-adjusted NO_x emissions on simulated NO_x and O_3 discrepancies in the urban and outflow areas of the Pacific and Lower Middle US, Atmospheric Chemistry and Physics, 14, 675-690.

Choi, Y., Kim, H., Tong, D., Lee, P. 2012: Summertime weekly cycles of observed and modeled NO_x and O_3 concentrations as a function of land use type and ozone production sensitivity over the Continental United States, Atmospheric Chemistry and Physics, 12, 6291-6307.

Crowley, J. N. and Carl, S. A.: OH Formation in the Photoexcitation of NO2 beyond the Dissociation Threshold in the Presence of Water Vapor, J. Phys. Chem. A, 101, 4178–4184, 1997.

Czader, B.H., X. Li, and B. Rappenglueck. 2013. CMAQ modeling and analysis of radicals, radical precursors and chemical transformations. J. Geophys. Res. doi: 10.1002/jgrd.50807, posted online: 5 Sep 2013.

Czader, B.H., B. Rappenglück, P. Percell, D. Byun, F. Ngan, and S. Kim. 2012. Modeling nitrous acid and its impact on ozone and hydroxyl radical during the Texas Air Quality Study 2006. Atmos. Chem. Phys. 12:6939–6951. doi: 10.5194/acp-12-6939-2012

Elshorbany, Y.F., R. Kurtenbach, P. Wiesen, E. Lissi, M. Rubio, G. Villena, E. Gramsch, A.R. Rickard, M.J. Pilling, and J. Kleffmann. 2009. Oxidation capacity of the city air of Santiago, Chile. Atmos. Chem. Phys. 9:2257–2273. doi:10.5194/acp-9-2257-2009

Finlayson-Pitts, B. J., Wingen, L. M., Sumner, A. L., Syomin, D. and Ramazan, K. A.: The heterogeneous hydrolysis of NO_2 in laboratory systems and in outdoor and indoor atmospheres: and integrated mechanism, Phys. Chem. Chem. Phys., 5, 223–242, 2003.

Foley, K. M., Roselle, S. J., Appel, K. W., Bhave, P. V., Pleim, J. E., Otte, T. L., Mathur, R., Sarwar, G., Young, J. O., Gilliam, R. C., Nolte, C. G., Kelly, J. T., Gilliland, A. B., and Bash, J. O.: Incremental testing of the Community Multiscale Air Quality (CMAQ) modeling system version 4.7, Geosci. Model Dev., 3, 205–226, doi:10.5194/gmd-3-205-2010, 2010.

George, C., Sterkowski, R. S., Kleffmann, J., Stemmler, K., and Ammann, M.: Photoenhanced uptake of gaseous NO_2 on solid organic compounds: a photochemical source of HONO?, Faraday Discuss., 130, 195–210, 2005.

Harris, G.W., W.P.L. Carter, A.M. Winer, J.N. Pitts, U. Platt, D. Perner: Observations of nitrous acid in the Los Angeles atmosphere and implications for the predictions of ozone-precursor relationships, Environ. Sci. Technol., 16, 414-419, 1982.

Kim, S., VandenBoer, T.C., Young, C.J., Riedel, T.P., Thornton, J.A., Swarthout, B., Sive, B., Lerner, B., Gilman, J.B., Warneke, C., Roberts, J.M., Guenther, A., Wagner, N.L., Dubé, W.P.,

Williams, E., Brown, S.S., 2014: The Primary and Recycling Sources of OH During the NACHTT-2011 Campaign-HONO as an important OH primary source in the wintertime. J. Geophys. Res. 119, 6886-6896, DOI:10.1002/2013JD019784

Kim, S.W., Heckel, A., Frost, G.J., Richter, A., Gleason, J., Burrows, J.P., McKeen, S., Hsie, E.-Y., Granier, C., and Trainer, M: NO_2 columns in the western United States observed from space and simulated by a regional chemistry model and their implications for NO_x emissions, J. Geophys. Res., 114, D11301, doi:10.1029/2008JD011343, 2009.

Kim, S.W., McKeen, S.A., Frost, G.J., Lee, S.-H., Trainer, M., Richter, A., Angevine, W.M., Atlas, E., Bianco, L., Boersma, K.F., Brioude, J., Burrows, J.P., de Gouw, J., Fried, A., Gleason, J., Hilboll, A., Mellqvist, J., Peischl, J., Richter, D., Rivera, C., Ryerson, T., Hekkert, S., Walega, J., Warneke, C., Weibring, P., and Williams, E.: Evaluation of NO_x and highly reactive VOC emission inventories in Texas and their implications for ozone plume simulations during the Texas Air Quality Study 2006, Atmos. Chem. Phys., 11, 11361-11386, doi:10.5194/acp-11-11361-2011, 2011.

Kirchstetter, T.W., R.A. Harley, and D. Littlejohn. 1996. Measurement of nitrous acid in motor vehicle exhaust. Environ. Sci. Technol. 30:2843–2849.doi:10.1021/es960135y

Kleffmann, J.: Daytime Sources of Nitrous Acid (HONO) in the Atmospheric Boundary Layer, Chem. Phys. Chem., 8, 1137–1144, doi:10.1002/cphc.200700016, 2007.

Kleffmann, J., Becker, K. H., and Wiesen, P.: Heterogeneous NO_2 conversion processes on acid surfaces: possible atmospheric implications, Atmos. Environ., 32, 2721–2729, 1998.

Kleffmann, J., Gavriloaiei, T., Hofzumahaus, A., Holland, F., Koppmann, R., Rupp, L., Schlosser, E., Siese, M., and Wahner, A.: Daytime formation of nitrous acid: A major source of OH radicals in a forest, Geophys. Res. Lett., 32, L05818, doi:10.1029/2005GL022524, 2005.

Kurtenbach, R., K.H. Becker, J.A.G. Gomes, J. Kleffmann, J.C. Lörzer, M. Spittler, P. Wiesen, R. Ackermann, A. Geyer, and U. Platt. 2001. Investigations of emissions and heterogeneous formation of HONO in a road traffic tunnel. Atmos. Environ. 35:3385–3394. doi:10.1016/S1352-2310(01)00138-8

Lefer, B., and B. Rappenglück (2010), The TexAQS-II radical and aerosol measurement project (TRAMP), Atmos. Environ., 44, 3997‑4004.

Li, S., Matthews, J., and Sinha, A.: Response to Comment on "Atmospheric Hydroxyl Radical Production from Electronically Excited NO_2 and H_2O", Science, 324, 336, doi:10.1126/science.1166877, 2009.

Li, S., Matthews, J., and Sinha, A.: Atmospheric Hydroxyl Radical Production from Electronically Excited NO_2 and H_2O, Science, 319, 1657–1660, 2008.

Li, Y., An, J., Min, M., Zhang, W., Wang, F., Xie, P., 2011: Impacts of HONO sources on the air quality in Beijing, Tianjin, and Hebei Province of Chaina. Atmospheric Environment, 45, 4735-4744.

Mao, J., X. Ren, S. Chen,W.H. Brune, Z. Chen, M. Martinez, H. Harder, B. Lefer, B. Rappenglück, J. Flynn, and M. Leuchner. 2010. Atmospheric oxidation capacity in the summer

of Houston 2006: Comparison with summer measurements in other metropolitan studies. Atmos. Environ. 44:4107–4115. doi: 10.1016/j.atmosenv.2009.01.013

Olaguer, E. P., C. E. Kolb, B. Lefer, B. Rappenglück, R. Zhang, and J. P. Pinto (2013), Overview of the SHARP campaign: motivation, design, and major outcomes, J. Geophys. Res. Atmos., 118, 5018‐5028, doi:10.1002/jgrd.50423.

Pagsberg, P., Bjergbakke, E., Ratajczak, E., and Sillesen, A.: Kinetics of the gas phase reaction OH + NO(+M)→HONO(+M) and the determination of the UV absorption cross section of HONO, Chem. Phys. Lett., 272, 383–390, 1997.

Perner, D., U. Platt: Detection of nitrous acid in the atmosphere by differential optical absorption, Geophys. Res. Lett., 6, 917-920, 1979.

Rappenglueck, B., Lubertino,G., Alvarez, S., Golovko, J., Czader, B., Ackermann, L.: Radical precursors and related species from traffic as observed and modeled at an urban highway junction, Journal of the Air & Waste Management Association, 63:11, 1270-1286, DOI: 10.1080/10962247.2013.822438, 2013.

Sarwar, G., Roselle, S. J., Mathur, R., Appel,W., Dennis, R. L., and Vogel, B.: A comparison of CMAQ HONO predictions with observations from the Northeast Oxidant and Particle Study, Atmos. Environ., 42, 5760–5770, 2008.

Skamarock,W. C., and Klemp, J. B.: A time-split non-hydrostatic atmospheric model for weatherresearch and forecasting applications, J. Comput. Phys.,227,3465–3485, 2008.

Stemmler, K., Ammann, M., Donders, C., Kleffmann, J., and George, C.: Photosensitizied reduction of nitrogen dioxide on humic acid as a source of nitrous acid, Nature, 440, 195–198, 2006.

Stemmler, K., Ndour, M., Elshorbany, Y., Kleffmann, J., D'Anna, B., George, C., Bohn, B., and Ammann, M.: Light induced conversion of nitrogen dioxide into nitrous acid on submicron humic acid aerosol, Atmos. Chem. Phys., 7, 4237–4248, doi:10.5194/acp-7-4237-2007, 2007.

Wong, K.W., Tsai, C., Lefer, B., Grossberg, N., Stutz, J., 2013: Modeling of daytime HONO vertical gradients during SHARP 2009. Atmos. Chem. Phys., 13, 3587-3601.

Willmott CJ. 1981: On the validation of models. Physical Geography 2: 184 – 194

480 Table 1. EPA emission trends for NO_x (values reported in thousands of tons).

NO_x	**2008**	**2009**	**2010**	**2011**	**2012**	**2013**
mobile	6,941	6,241	5,734	5,786	5,398	5,010
other	9,872	9,540	9,144	8,594	8,114	7,914
total	**16,813**	**15,781**	**14,878**	**14,380**	**13,512**	**12,924**

481

482

Table 2. Summary of statistical parameters for the base case simulation (B) and reduced NO_x case (N).

Site	No. of points	Mean (ppb)			R		AME (ppb)		IOA	
		Obs.	Sim. B	Sim. N	Sim. B	Sim. N	Sim. B	Sim. N	Sim. B	Sim. N
1	700	15.60	18.95	12.41	0.44	0.45	10.52	8.18	0.62	0.58
2	695	6.34	9.13	5.42	0.49	0.54	5.39	3.62	0.54	0.70
8	699	9.93	11.89	8.24	0.73	0.76	5.45	4.53	0.83	0.84
9	699	5.50	10.02	6.54	0.60	0.59	5.66	3.74	0.66	0.74
15	668	10.48	12.98	7.92	0.42	0.44	8.20	6.26	0.61	0.56
26	697	5.61	12.58	9.58	0.52	0.56	7.96	5.45	0.47	0.61
35	649	6.63	10.33	6.95	0.67	0.64	5.87	3.93	0.72	0.79
45	699	3.83	4.87	3.45	0.60	0.52	2.94	2.42	0.72	0.70
53	684	7.69	11.56	8.80	0.76	0.77	5.74	4.28	0.82	0.87
64	690	4.01	2.51	1.91	0.44	0.54	2.72	2.57	0.61	0.57
78	617	3.29	10.45	7.56	0.54	0.55	7.66	5.01	0.41	0.54
84	533	4.34	9.08	6.88	0.69	0.70	5.57	3.82	0.68	0.78
114	708	13.94	20.87	13.79	0.48	0.50	11.44	7.54	0.62	0.68
311	635	4.58	6.75	4.92	0.52	0.58	3.74	2.70	0.66	0.75
403	696	14.87	27.20	20.08	0.40	0.42	16.40	11.83	0.54	0.61
408	703	15.17	12.01	8.90	0.55	0.59	7.08	7.74	0.67	0.61
411	692	16.57	22.24	15.81	0.59	0.60	10.59	7.87	0.69	0.76
416	702	13.95	28.35	19.43	0.71	0.71	16.39	9.29	0.69	0.81
617	705	6.20	7.42	4.93	0.50	0.48	4.50	3.61	0.64	0.68
618	697	2.90	3.15	1.80	0.58	0.61	1.62	1.42	0.71	0.71
619	559	3.04	2.38	1.67	0.38	0.48	2.34	2.01	0.58	0.58
620	399	7.05	7.66	4.86	0.37	0.36	6.74	5.67	0.57	0.49
640	675	2.14	1.57	1.10	0.26	0.30	1.50	1.36	0.47	0.47
643	671	6.30	1.82	1.35	0.21	0.24	4.97	5.15	0.46	0.44
1015	703	13.44	12.33	8.75	0.43	0.44	8.95	8.65	0.62	0.56
1016	608	2.25	5.18	3.73	0.40	0.40	3.55	2.50	0.48	0.57
1034	641	2.23	1.58	1.38	0.45	0.47	1.43	1.39	0.63	0.60
1035	692	4.45	7.91	5.12	0.53	0.55	4.49	2.96	0.64	0.74
1628	630	5.91	13.64	5.09	0.43	0.50	8.39	2.98	0.42	0.69
MT	703	9.93	20.53	14.59	0.64	0.64	12.46	8.02	0.63	0.74
ALL	**19849**	**7.76**	**11.11**	**7.59**	**0.58**	**0.59**	**6.76**	**4.94**	**0.71**	**0.75**

Table 3. Statistical parameters for modeling HONO mixing ratios for the Moody Tower site.

Statistics		HONO
Number of points		200
Mean	Observed	0.69
	Sim. (N)	0.30
	Sim. (NH)	0.41
Max. value	Observed	3.15
	Sim. (N)	2.62
	Sim. (NH)	2.93
Correlation coefficient	Sim. (N)	0.58
	Sim. (NH)	0.57
Mean Bias	Sim. (N(	-0.39
	Sim. (NH)	-0.28
Absolute Mean Error	Sim. (N)	0.46
	Sim. (NH)	0.43
Index of agreement	Sim. (N)	0.63
	Sim. (NH)	0.70

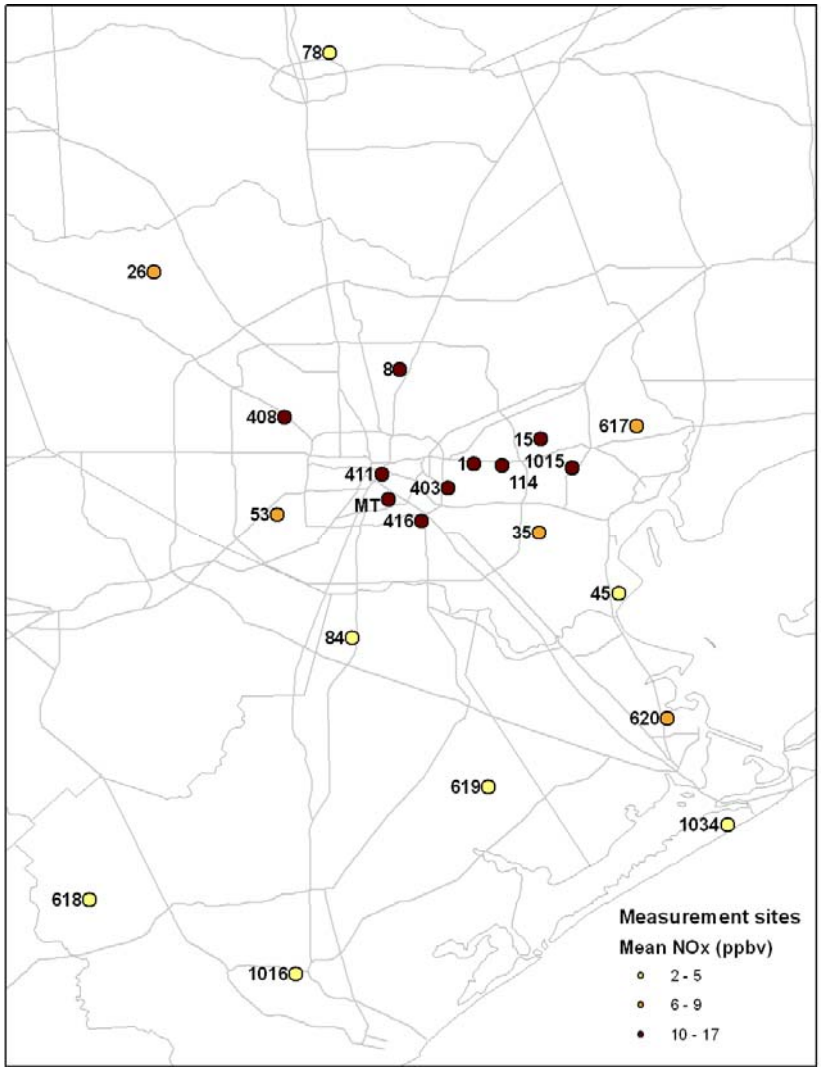

491

492 Figure 1. Locations of stations performing NO_x measurements in the Houston-Galveston-

493 Brazoria area during September 2013.

494

495

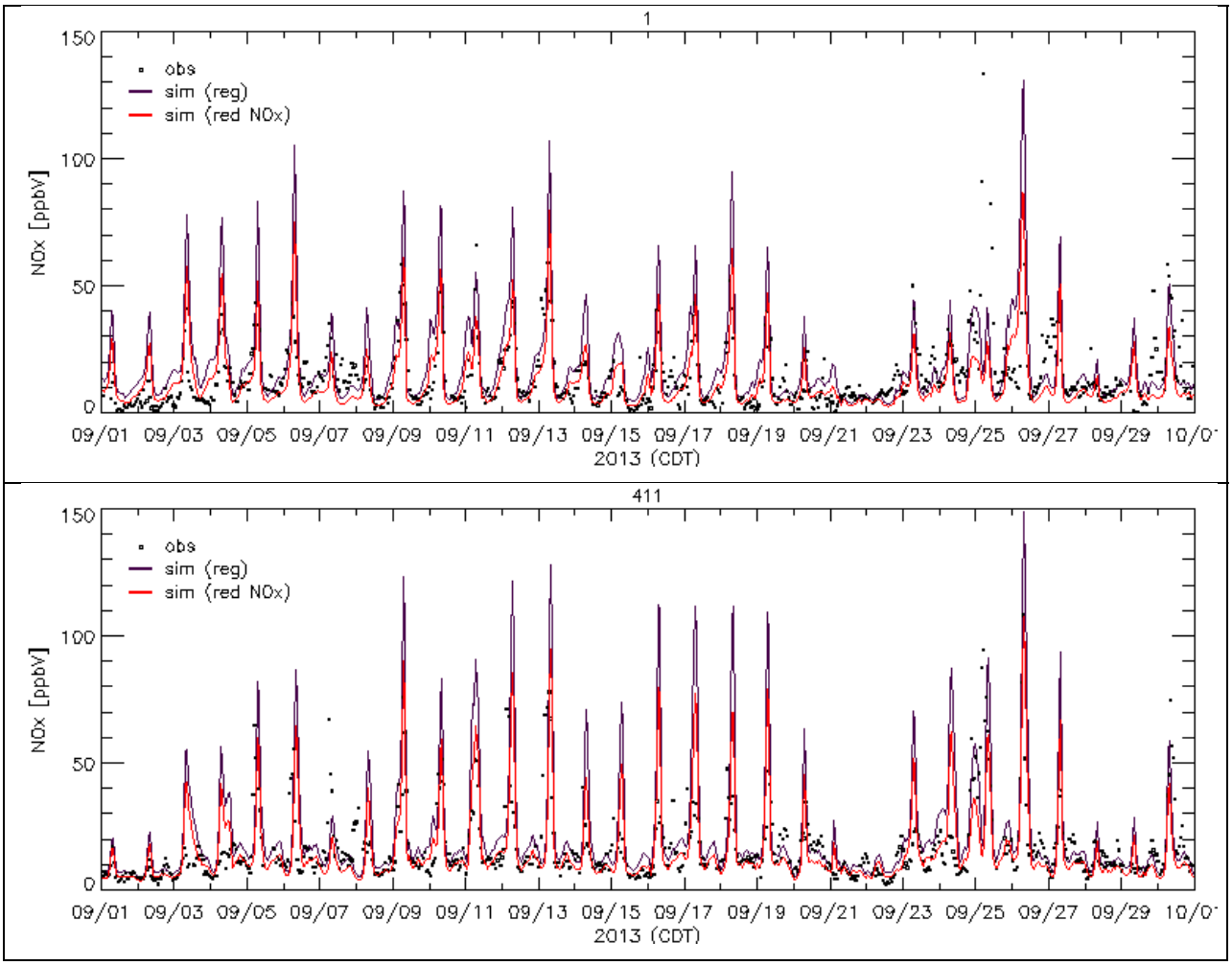

Figure 2. Timeseries comparing measured NO_x against values simulated with the base case and the reduced NO_x case at CAMS sites 1 and 411.

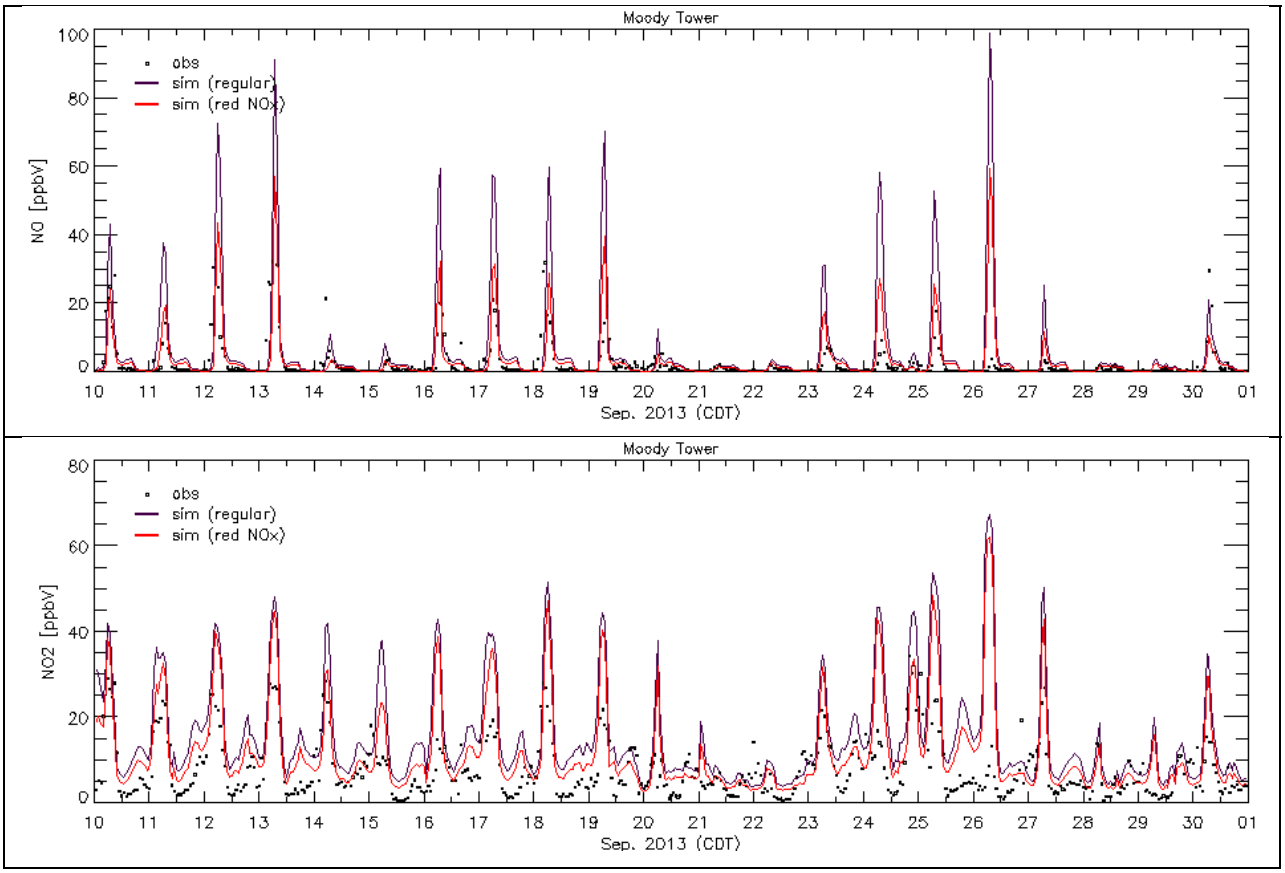

501 Figure 3. NO and NO_2 mixing ratio measured at the Moody Tower site and modeled with the
502 base case emissions as well as with reduced NO_x emissions.

503

504

505

506

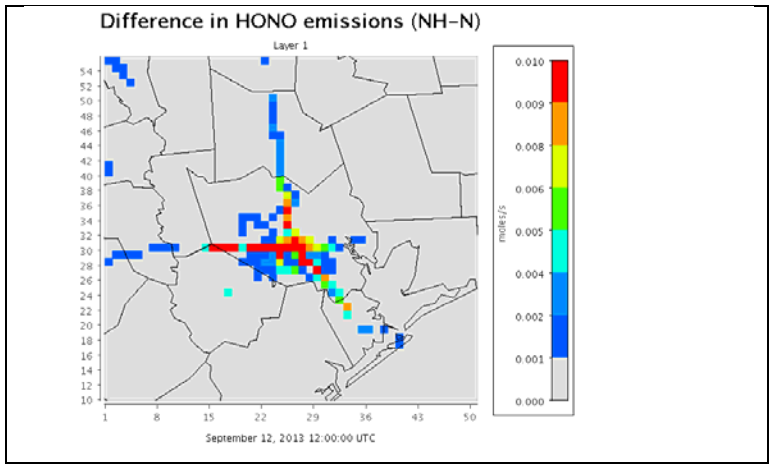

507 Figure 4. Snapshot of differences in HONO emissions between a case with emission ratio of
508 $HONO/NO_x$ =0.016 (NH) and default emissions of $HONO/NO_x$=0.008 (N) at 7 a.m. LT on
509 September 12, 2013.

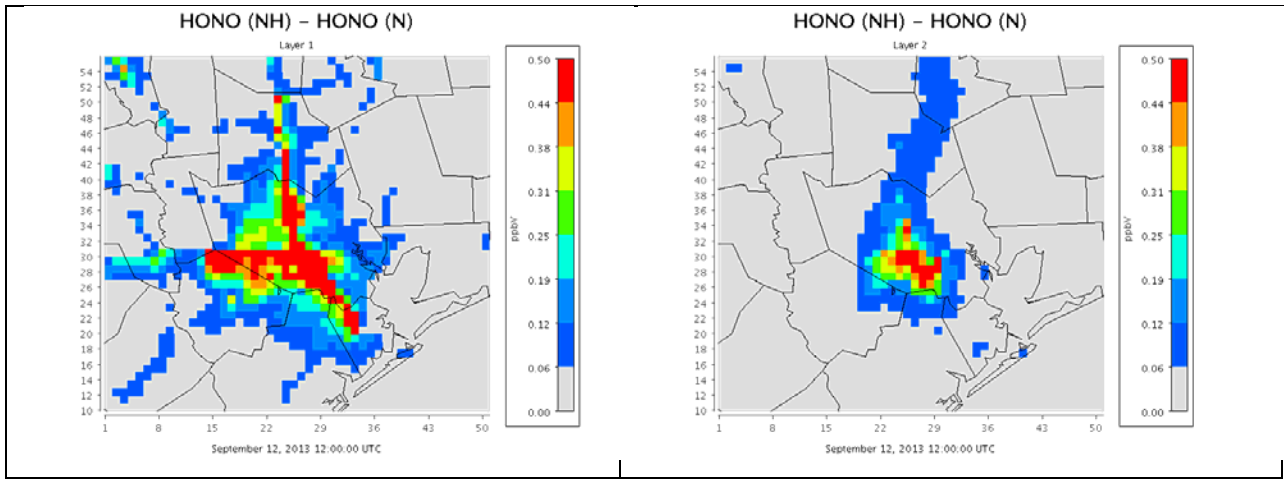

510 Figure 5. Differences in HONO mixing ratios between a case with 0.016 $HONO/NO_x$ emission
511 ratio (NH) and 0.008 $HONO/NO_x$ emissions (N) for the surface (left) and the second model layer
512 (right) at 7 a.m. LT on September 12, 2013.

513

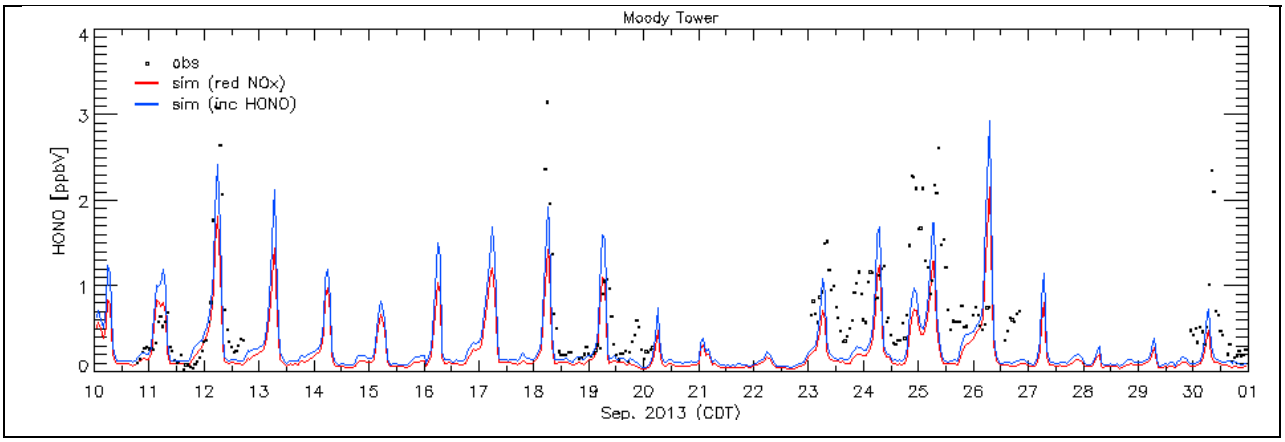

514 Figure 6. HONO mixing ratios measured at the Moody Tower site and modeled with and the
515 regular HONO emissions (N) for which the HONO/NO_x emission ratio of 0.008 was used, and
516 the increased HONO case (NH) for which the HONO/NO_x emission ratio of 0.016 was used.

517

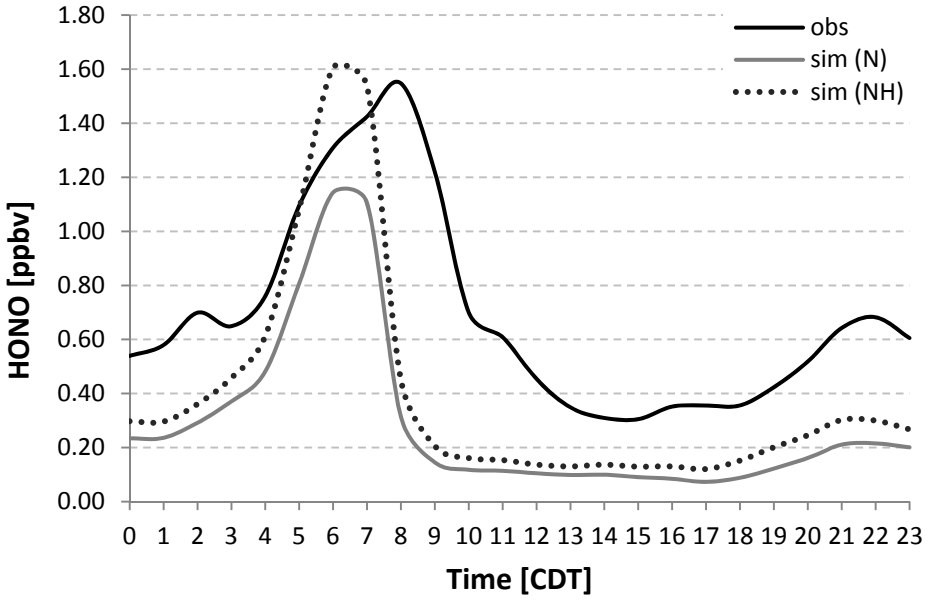

Figure 7. Average diurnal variation of HONO at the Moody Tower measurement site.

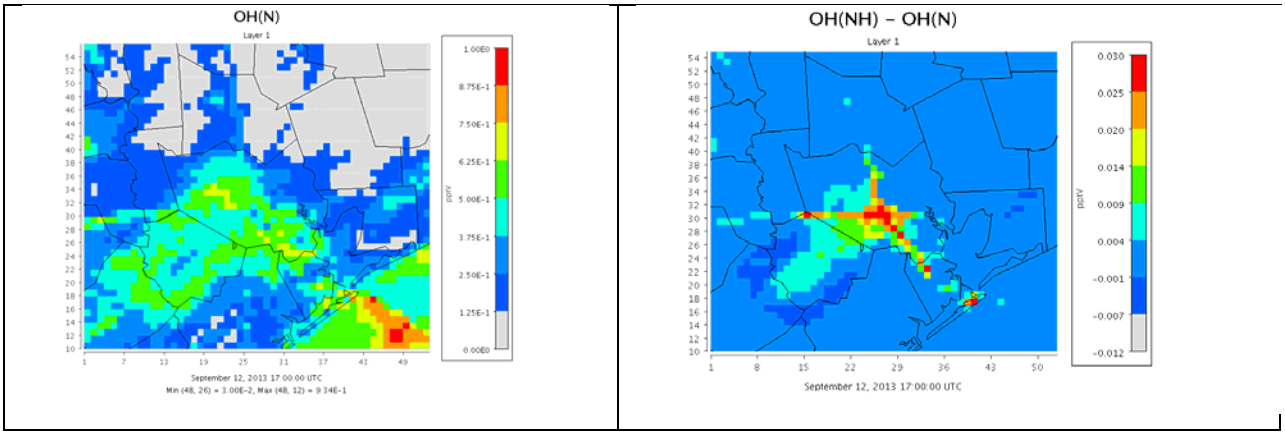

Figure 8. OH mixing ratios (left) and differences in OH mixing ratios (right) between the case with 0.008 HONO/NO_x emission ratio (N) and 0.016 HONO/ NO_x emission ratio (NH) at noon local time on September 12, 2013.

527

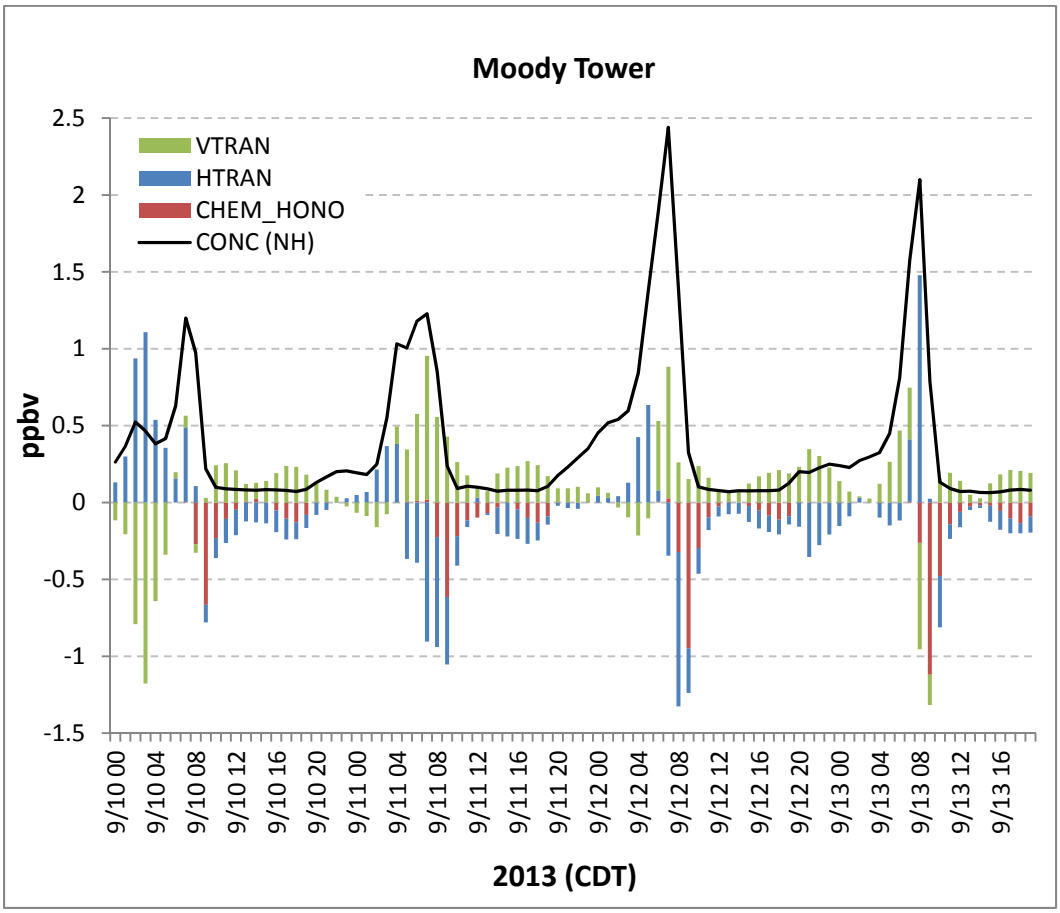

528

529 Figure 9. HONO mixing ratios (black line) and processes contributing to changes in HONO
530 mixing ratio at the Moody Tower site where the measurements were taken, which corresponds to
531 the second model layer, where VTRAN is vertical transport, HTRAN is transport in horizontal
532 direction, and CHEM_HONO correspond to changes due to chemical reactions.